Materialia 9 (2020) 100609

Contents lists available at ScienceDirect

Materialia

journal homepage: www.elsevier.com/locate/mtla

Full Length Article

Guided bone marrow stimulation for articular cartilage repair through a freeze-dried chitosan microparticle approach

Caroline D. Hoemann[a,b,c,*], Jessica Guzmán-Morales[a], Geneviève Picard[a], Gaoping Chen[a], Daniel Veilleux[a], Anik Chevrier[a], Sotcheadt Sim[a,d], Martin Garon[d], Eric Quenneville[d], Charles-Hubert Lafantaisie-Favreau[a], Michael D. Buschmann[a,b,c], Mark B. Hurtig[e]

[a] Department of Chemical Engineering, Polytechnique Montreal, QC, Canada
[b] Institute of Biomedical Engineering, Polytechnique Montreal, QC, Canada
[c] Bioengineering Department, George Mason University, 10920 George Mason Circle, Manassas, VA 20110, USA
[d] Biomomentum Inc, Laval, QC, Canada
[e] Department of Clinical Studies, University of Guelph, Guelph, ON, Canada

ARTICLE INFO

Keywords:
Articular cartilage repair
Biomaterials
Bone remodeling
Animal models
Structural stiffness
Angiogenesis

ABSTRACT

A novel approach for stimulating articular cartilage repair was developed and evaluated in skeletally aged Arcott sheep with signs of early osteoarthritis. Freeze-dried (FD) chitosan formulations were optimized to produce ultraporous cylinders that slowly rehydrate and disperse into bioactive chitosan microparticles in coagulating blood plasma. FD-chitosan implants (80% Degree of Deacetylation, 85 kDa) were produced at 3 doses (initial concentrations of 5, 10, 20 mg/mL, pH 2.5). Full-thickness cartilage defects were created bilaterally in medial femoral condyles of 8–9 year-old sheep ($N = 12$), microdrilled with 11 holes, then in one knee per sheep, one implant cylinder was inserted into each bleeding drill hole. At 1 day ($N = 2$), 3 months ($N = 5$) and 9 months ($N = 5$) post-operative, repair tissues were analyzed macroscopically and by micro-computed tomography, histology, biochemistry, and mechanics. Chitosan microparticles were detected in day 1 subchondral blood clots and mostly cleared at 3 months. At 3 months, microdrill holes were 2-fold larger, filled with angiogenic granulation tissue, callus, and woven bone, with more chondroinduction in treated *versus* control drill holes ($p = 0.021$). At 9 months, biomaterial treatment enhanced bone plate repair and stimulated 68% cartilage resurfacing *vs* 53% for drill-only controls ($p = 0.047$). Both treated and control cartilage repair tissues had lower glycosaminoglycan content than intact cartilage and were thinner, stiffer, and more permeable. Upon indentation, hyaline-like repair cartilage showed poroelastic behavior. This study showed that FD-chitosan can be locally delivered to incorporate chitosan microparticles into subchondral bone blood clots and exert anabolic therapeutic effects on articular cartilage resurfacing in aged sheep knees.

1. Introduction

Bone marrow stimulation (BMS) is a surgical technique currently used to treat focal articular cartilage lesions. Microfracture has a therapeutic benefit for most patients who report less pain and improved function at 2 years post-operative [1,2] however after 15 years post-operative, a microfracture cohort showed a 32.5% failure rate [3]. Current evidence suggests that some procedures fail because the subchondral bone holes produce less cartilage repair tissue in patients over 35 years old [2,4,5]. As most patients with cartilage lesions are over 40 years old, effective cartilage repair therapy for aged patients remains an undisputed unmet need in orthopedics [6]. During the bone marrow stimulation procedure, the surgeon debrides all residual lesional cartilage along with the underlying calcified cartilage layer, then perforates small holes in the exposed subchondral bone with an awl, drill or K-wire [7–10]. This controlled bone damage elicits bone bleeding and stimulates a bone marrow-driven wound healing response. In ideal cases, exposed bone becomes resurfaced with a hyaline-like

Abbreviations: BMS, bone marrow stimulation; DDA, Degree of Deacetylation; EDTA, ethylene diamine tetra acetic acid; FD, freeze-dried; IV, intravenous; kDa, kilodalton; micro-CT, micro-computed tomography; mOsm, milliosmole; RITC, rhodamine isothiocyanate; SafO, Safranin O; SEC-MALS, molecular weight by size exclusion chromatography-multi-angle light scattering; sGAG, sulfated glycosaminoglycan; SMS, subchondral marrow stimulation.

* Corresponding author at: Bioengineering Department, George Mason University, 10920 George Mason Circle, Manassas, VA 20110, USA.
E-mail address: choemann@gmu.edu (C.D. Hoemann).

https://doi.org/10.1016/j.mtla.2020.100609
Received 19 November 2019; Accepted 29 January 2020
Available online 4 February 2020

cartilage tissue, but most frequently the repair site is filled with a mixture of hyaline-like cartilage, fibrocartilage or fibrous tissue, with some treated lesions persisting as exposed bone, for reasons that remain unclear [11,12].

Augmented microfracture is a concept based on the premise that a device or biologic can be used to elicit a more voluminous, hyaline-like cartilage repair tissue from lesions treated by BMS [13]. One augmentation approach intends to fill the osteochondral wound void with a solid substrate with or without added cells [14–17]. However, animal model testing has revealed that the longer a scaffold persists in the lesion, the worse the repair outcome is observed compared to surgery alone [17–23]. The conceptual framework of this study arose from emerging evidence that subchondral bone plate remodeling (*i.e.*, bone damage, resorption and repair) can give rise to chondroinduction followed by articular cartilage regeneration [24–29]. Chondroinduction arises through as-yet undetermined mechanisms that trigger the formation of chondrogenic foci at the osteochondral junction, and this is distinct from premature cartilage formation in the subchondral bone that subsequently mineralizes and is known as a callus. Chondroinduction can be elicited to various degrees in animal models by different biomaterial implants that support subchondral bone plate regeneration [26,28,30]. However subchondral bone sclerosis can develop in older patients with chronic lesions and this can mute the bone remodeling response and physically obstruct bone marrow cell migration towards the cartilage lesion [31,32]. One way to overcome this barrier would be to deliver a bone-remodeling implant directly into subchondral bone marrow stimulation channels [33]. This approach is termed “subchondral marrow stimulation” (SMS).

Chitosan is a biodegradable polysaccharide that can enhance wound-repair through its bioactive effects on the innate immune response. Chitosans containing ~80% glucosamine and ~20% N-acetyl glucosamine, in the form of microparticles, attract more neutrophils, macrophages, blood vessels, and osteoclasts to osteochondral defects [30,34]. Osteoclast activity at the bone plate induces bone remodeling and attracts mesenchymal stem cells that can subsequently undergo chondroinduction at the base of the cartilage lesion [30]. For cartilage repair applications, chitosan microparticles are preferred over solid scaffolds or hydrogels, because microparticles have a more controlled clearance rate than solid chitosan scaffolds whose physical forms can persist in the wound and block angiogenic bone repair [23]. Presolidified chitosan/blood implants containing rapidly degrading 10 kDa chitosan particles were previously shown to improve cartilage repair in skeletally aged rabbits [27], but a device has yet to be identified that improves cartilage repair in a skeletally aged large animal model.

The purpose of this study was to create an off-the-shelf device that improves cartilage resurfacing in a skeletally aged large animal model. A freeze-dried (FD) chitosan implant was therefore designed to disperse as microparticles in coagulating blood, because biodegradable chitosan microparticles were previously shown to stimulate sterile inflammatory angiogenesis and bone remodeling in *in vivo* cartilage repair models [30], and more hyaline repair cartilage *versus* drilling alone [27].

In the first phase of this study, we screened over 40 FD-chitosan formulations *in vitro* with and without different lyoprotectants (sucrose, trehalose, dextran, sorbitol), at distinct pH and chitosan concentrations. Lyoprotectants were added to enhance rigidity of the chitosan cake and to facilitate rehydration and dispersion of chitosan into microparticles in coagulating blood plasma. This approach is in contrast to other chitosan scaffolds that are intended to remain as a solid scaffold after implanting in a wound [23,35,36]. After screening 5 optimized formulations in an *in vivo* rabbit model, one formulation was selected for testing in an SMS model with 12 skeletally aged sheep that, at 8 to 9 years old, have signs of early osteoarthritis. We tested the hypotheses that FD-chitosan implant resides as microparticles in the drill hole subchondral blood clot, elicits bone remodeling and chondroinduction at 3 months post-operative, and enhances poroelastic hyaline repair at 9 months *versus* microdrilling-alone.

2. Materials and methods

2.1. Materials

Chitosans of different Degree of Deacetylation (DDA) and molecular weight were produced in-house from Marinard starting material (NB, Canada) and purified by alkaline precipitation. Chitosans were characterized for DDA by ^{1}H NMR and for molecular weight by size exclusion chromatography-multi-angle light scattering (SEC-MALS) (Table 1). Rhodamine isothiocyanate (RITC) covalently coupled to chitosan at 1% mol/mol was prepared as described [37]. Reagents purchased from Sigma-Aldrich (Oakville, ON) included $CaCl_2$ dihydrate (#C7902), 1 N cell culture-grade HCl (#H9892) and lyoprotectants: sucrose (#037K01071), trehalose (#020m70073v), sorbitol (#019k013320), D-glucosamine-HCl (#125k00241), N-acetyl glucosamine (#099k00813v); dextran-5 was from Pharmacosmos A/S (#HK2171). Chitosan dissolved in dilute HCl was autoclave-sterilized, diluted with sterile ddH_20 to concentrations from 2.4 to 20 mg/mL at different pH levels (pH 2.5 to 6.0), without or with filter-sterilized lyoprotectant (2.5–50 mg/mL), dispensed as 0.5 mL aliquots in sterile glass vials then freeze-dried aseptically in a Laboratory Series Programmable logic controller (PLC) Stoppering Freeze-Dryer (Model LD85S3, Millrock Technologies Inc., −40 °C, 100 mTorr for 48 h). Selected samples were freeze-dried in a standard Freezone 12-port Freeze Dry System (LabConco). Sphericel® glass microbeads (Grade 110P8) were from Matweb.

2.2. In vitro *formulation screening*

The ability of different FD-chitosan scaffold formulations to rehydrate and disperse into microparticles in a fibrin clot was evaluated in a human citrated blood plasma coagulation assay with a controlled 12-min coagulation time [38]. FD-chitosan scaffold containing a fluorescent RITC-chitosan tracer with matching DDA and molecular weight (weighing ~0.5 mg) was freeze-dried (Millrock), then a core was extracted with a 1.5 mm biopsy punch, and submerged in 170 μL citrated human blood plasma containing clot activator (10 μL 200 mM $CaCl_2$ and 5 μL 10 mg/mL glass microbead suspension in ddH_20) for 1 h at 37 °C in a 96-well plate to allow fibrin clot formation. Microparticle dispersion was documented by epifluorescence microscopy, capturing digital images with controlled exposure time and fluorescence intensity.

2.3. Animal study design and testing

All animal procedures were approved by institutional ethics review boards and in conformity with ARRIVE guidelines [39].

2.3.1. Pilot rabbit screening

Skeletally immature New Zealand White rabbits (N = 4 male) were randomly assigned drill hole treatment condition with 2 days (N = 1) or 21 days (N = 3) of repair. Rabbits were given a fentanyl patch the day prior to surgery for analgesia, fully anesthetized with ketamine-xylazine and maintained with isoflurane/oxygen. Sequential mini-arthrotomies were used to create 2 osteochondral drill holes, 2 mm deep in the trochlear groove with a 1.4 mm stainless steel drill burr (Fine Science Tools, catalog No. 19,007–14). Drill holes were left to bleed (control) or treated by inserting in the proximal hole a 1.5 mm diameter cored cylinder of FD-lyoprotectant (50 mg/mL initial concentration of sucrose, sorbitol, trehalose, dextran-5), and in the distal hole a cored cylinder of FD-chitosan (2.4, 5 or 10 mg/mL initial chitosan concentration, with 0.1% w/w rhodamine-isothiocyanate-chitosan tracer) without or with 50 mg/mL initial concentration of lyoprotectant (Table 1). Knees were closed in 3 sutured layers. Rabbits were euthanized by IV pentobarbital under full anesthesia. Distal femurs were formalin-fixed, scanned by micro-computed tomography, EDTA-decalcified and cryosectioned with CryoJane tape. Sections were histostained with SafraninO/Fast Green

Table 1
Characteristics of the chitosan solutions used in the *in vivo* studies prior to freeze-drying.

Chitosan	lot number	DDA	Mn	Mw	PDI	Concentration (Osmolality)
Rabbit study						
80–10K	10K03	81.9	25,100	7451	3.37	20 mg/mL (77 mOsm)
RITC-10 K (a)	CHEM5575	81.9	22,400	12,400	1.8	0.125 mg/mL (N.R.)
Sheep study						
80–85K	80M8	80.6	85,380	52,590	1.62	20 mg/mL (46 mOsm) 10 mg/mL (25 mOsm) 5 mg/mL (10 mOsm)
RITC-80M4 (b)	CHEM4956	81.8	246,400	176,000	1.4	0.125 mg/mL (N.R.)

Fluorescent chitosan tracer (a) 0.6% mol/mol RITC/chitosan or (b) 0.5% mol/mol RITC/chitosan was added to the chitosan solution prior to FD, and contributed non-relevant (N.R.) levels of osmolality to the formulation.

(Saf-O) or Gomori Trichrome, or enzymatically digested with pronase and hyaluronidase, and immunostained for collagen type I (I-8H5 monoclonal 1:100 dilution, Calbiochem, Product No. CP-17), biotinylated goat anti-mouse IgG (Vector, lot V0609) and ABC-AP red detection.

2.3.2. Sheep model of subchondral marrow stimulation

Arcott cross sheep (8–9-year-old $N = 12$, females, 66 ± 6 kg) from specific pathogen-free herds were randomized to implant-treated knee (left *vs* right), and day 1 ($N = 2$), 3 months ($N = 2$) and 9 months ($N = 8$) of repair. Sheep were anesthetized with intravenous ketamine and diazepam and then maintained on isoflurane gas. Sequential mini-arthrotomies were used to access the joint surface of both knees and a curette used to create a full-thickness ≈15 × 10 mm chondral defect debrided of the superficial calcified layer in the load-bearing area of each medial femoral condyle. A 1.4 mm diameter microburr was used to perforate 11 microdrill holes at a 2 mm target depth in 3 vertical (proximal-to-distal) rows of 3 or 4 holes with constant irrigation with saline. The surgeon transferred FD-chitosan cylinders to individual drill holes in one knee with a sterile tweezers, with a distinct dose (chitosan-HCl initial concentration 5, 10, and 20 mg/mL, pH 2.5) for each of the 3 proximal-to-distal rows, a total of ~2 mg of chitosan per condyle. Control drill holes in the contralateral knee were left to bleed without treatment. Animals received analgesic medication after surgery. Sheep were housed in groups in 3 × 4 m stalls post-operatively for one week, and then permitted access to larger pens with a good footing. All sheep experienced acute post-operative lameness that subsided by 2 months except for 3 sheep in the 9-month group that had persisting lameness and were reallocated to the 3-month group and euthanized at 3 months. No unscheduled deaths occurred in the experiment. Sheep were euthanized after 1 day ($N = 2$), 3 months ($N = 5$), and 9 months ($N = 5$) for osteochondral tissue analyses.

2.3.3. Sheep defect macroscopic assessment, micro-CT scanning, and histostaining

At necropsy, cartilage repair sites were photo-documented with a digital camera. The surface of day 1 and 3 month repair tissues were imaged by epifluorescence microscopy at 1.25× magnification. Menisci were frozen, and scored for degeneration from digital images [40] on a scale of 0 (smooth), 1 (slight fibrillation), 2 (moderate fibrillation, partial tears), 3 (complete tears), 4 (severe disruption). Distal 9 month repaired femoral ends were dissected, submitted to indentation measures in a saline bath, after which Jamshidi needle biopsies and full-thickness cartilage shavings were recovered from the distal repaired defect, and outside the defect area in the lateral femoral condyle (LFC), for mechanical testing and biochemical assays of glycosaminoglycan [41]. Medial femoral condyle defect samples were fixed in 4% paraformaldehyde/0.1 M cacodylate and scanned by microcomputed tomography (micro-CT, Skyscan X-ray Microtomography 1172, Kontich, Belgium) at 15 μm resolution, 80 kV, with Al–Cu filter and an image pixel size of 12.9 μm, decalcified in 0.5 N HCl/0.1% glutaraldehyde/ PBS at 4 °C, cut transversely in to 3 sagittal blocks, and embedded in paraffin to generate 6 μm serial sections through three areas in the middle of each row of holes. Calibrated line measures (Northern Eclipse) in macroscopic images of trimmed blocks were used to measure the distance of trimming needed to attain the middle of each row of holes. Sections were stained with Saf-O, Hematoxylin-Eosin and Gomori Trichrome and digitally scanned at 40x magnification (NanoZoomer-RS, Hamamatsu Photonics, Hamamatsu City, Japan) for quantitative histomorphometry and histological scoring using NDP view software.

2.3.4. Quantification of macroscopic percentage resurfacing

Macroscopic percent defect fill with repair tissue was determined from digital images of the 9-month defects obtained at necropsy. Regions of interest (ROIs) were defined as the total defect area, and the defect area covered by white smooth soft tissue (excluding visible pale yellow exposed bone). ROIs were measured by 2 blinded readers using the Northern Eclipse (Empix Imaging Inc., Mississauga, ON) polygon tool (pixels as measure units). Percentage resurfacing was calculated as the soft repair tissue area divided by the total defect area.

2.3.5. Micro-CT analysis of repair bone

Micro-CT scanned datasets of day 1, 3-month and 9-month samples were reconstructed in a 3D model using NRecon (Skyscan software, smoothing 2, misalignment 0, ring artifact correction 4, beam hardening correction 30%). Blinded reconstructions were repositioned in order to vertically align the central hole of each condyle and then each residual drill hole was analyzed to measure non-mineralized drill hole cross-sectional area at the surface (top) and at −0.5 mm, −1.0 mm, −1.5 mm below the bone surface, and hole depth using CTAn and DataViewer software (SkyScan), as previously described [42]. Data were presented as the mean±standard error of the mean cross-sectional area at each depth for all microdrill holes in $N = 4$ condyles at day 1, in $N = 5$ condyles per group for 3 months and in $N = 5$ condyles per group for 9 months.

2.3.6. Quantitative histomorphometry and histological scoring

Semi-quantitative scoring of callus formation and chondroinduction in 3 month repair tissue was assessed by 2 blinded readers from Saf-O and Gomori-stained serial sagittal sections collected through the middle of the drill holes. Callus formation was scored as visible areas of Saf-O-stained tissue in the subchondral area (below 200 μm from the bone surface). Chondroinduction was scored by the presence of repair tissue at or above the osteochondral junction that stained red with Saf-O and contained cells with chondrocyte morphology (score of 1) as compared to no tissue, tissues devoid of Saf-O staining (angiogenic tissue, woven bone), or cartilage flow (score of 0). The percentage callus formation and chondroinduction was determined (11 holes, 5 defects, $N = 55$ per condition). Two trained and blinded readers measured the percent resurfacing of bone with integrated cartilage repair tissue and the percent exposed bone in the defect area of 3 Saf-O-stained sections per 9-month

repaired defect by measuring the sum of all calibrated line measures of integrated soft tissue or mineralized tissue, divided by defect width along a projected tidemark from the flanking cartilage (Northern Eclipse, Empix Imaging Inc., Mississauga, ON). ICRS II histologic scoring [43,44] was performed on 3 Saf-O and Hematoxylin-eosin sections per defect by 3 trained and blinded readers to generate mean ICRS-II scores (category/score: 1/tissue morphology; 2/matrix staining; 3/cell morphology; 4/chondrocyte clustering; 5/surface architecture; 6/basal integration; 7/tidemark formation; 8/subchondral bone abnormalities; 9/inflammation; 10/abnormal calcification; 11/vascularization; 12/surface or superficial assessment; 13/mid-deep zone assessment; 14/Overall assessment. In 11 out of 30 histology sections, repair cartilage was missing in focal areas where a biochemical biopsy or a mechanical biopsy was extracted, as determined by comparing histology sections with calibrated macroscopic images taken before and after biopsies were collected. When carrying out blinded histomorphometry for % integrated repair and the ICRS II category 14 Overall score, the biopsy sites were omitted from the scoring.

2.3.7. Mechanical tests

Freshly dissected femur ends from the 9 month repair group were placed in an isotonic saline bath to perform indentation measurements with a spherical indenter of 0.5 mm radius and a mechanical tester (3-axis Mach-1 v500css from Biomomentum Inc., Laval, QC, Canada). For each test site, the indenter was positioned ~2 mm above the cartilage surface, the indenter detected the cartilage surface at the test site and at four neighboring positions to calculate the surface angle, then the test site was indented perpendicularly for 0.2 mm at 0.2 mm/s. A digital camera was used to map the position of each test site (21–62 discrete measures for LFC and MFC per knee). Structural stiffness (SS, in N/mm) was calculated at 50, 100 and 150 μm of indentation depth. Jamshidi osteochondral biopsies were extracted from the distal repair tissue and intact LFC. Cartilage thickness of the biopsies was determined from calibrated line measures of digital images taken with a dissection microscope. Unconfined compression tests (stress relaxation using a pre-compression of 10% strain followed by 5 compressions of 2% strain at 0.4% strain rate) of Jamshidi biopsies were carried out with a Mach-1 (Biomomentum, Laval, QC) in an isotonic saline bath. A linear fibril-network-reinforced biphasic model [45] was used to fit the 2% strain stress relaxation ramps to determine the fibril modulus (Ef, MPa), matrix modulus (Em, MPa) and permeability (x10^{-12} m^4/N s).

2.4. Statistical analyses

1-tailed Student's *t*-test was used to test the effect of implant treatment on macroscopic % repair tissue fill. The General Linear Model (GLM) with Unequal N Honest Significant Differences (HSD) post-hoc analysis (Statistica, Statsoft, Tulsa, AR) was used to analyze differences in residual bone hole diameter with time (day 1, 3 and 9 months), treatment (yes-no), and hole depth (top, −0.5, −1.0, −1.5 mm) as categorical predictors and individual drill holes as the statistical unit (N = 33–45 per condition). The effect of treatment on 3 month chondroinduction or callus formation, and 9 month integrated soft tissue repair and exposed mineral tissue was analyzed by the GLM with a Tukey HSD post-hoc analysis. ICRS-II histological scores from 3 blinded readers for 3 histology sections per defect were averaged and the GLM used to assess differences (N = 5 treated, control). Site-specific differences in 9 month sGAG levels, cartilage thickness, mechanical properties (Em, Ef, permeability) and SS@100 μm were evaluated with JMP® (v14.1.0; SAS, Cary, NC). Significance was set at $p<0.05$.

3. Results

3.1. FD-chitosan formulation optimization

Chitosan solutions that were freeze-dried in a standard freeze-dryer produced large chitosan flakes whereas freeze-drying under controlled temperature and vacuum produced rigid, ultraporous chitosan cakes that could be shaped into cylinders with a biopsy punch (Fig. 1A and B).

To develop FD-chitosan formulations with good cake rigidity that dispersed as microparticles in coagulating blood plasma, FD-chitosan cakes were produced with different chitosan molecular weight, concentration and pH, with and without lyoprotectants (sucrose, trehalose, sorbitol, dextran-5). Lyoprotectants, or bulking agents, were added to obtain more rigid cakes and to promote chitosan rehydration. From these tests we discovered that FD-chitosan ≥pH 4.5 formulations failed to disperse into microparticles, even with added lyoprotectants (Fig. 1C and D). FD-chitosan formulations generated at pH 2.5, where all glucosamine free amine groups are fully protonated, formed rigid cakes, and spontaneously dispersed into microparticles when immersed in coagulating human blood plasma (Fig. 1E).

To select a formulation with good surgical handling properties, FD-chitosan implants were generated (10 kDa chitosan pH 2.5, ± different lyoprotectants to increase cake rigidity), and evaluated in an *in vivo* rabbit microdrill model of cartilage repair. In this model, microdrill defects slowly filled with blood. Drill-only control defects were filled with blood clot at day 2 post-operative and at day 21 contained fibrocartilage that was poorly integrated with non-remodeled bone (Fig. 1F–I). During the surgery, FD-chitosan implants containing lyoprotectant (sucrose, trehalose, or sorbitol) were rigid and easily manipulated as long as they remained dry, but the moment they came into contact with blood in the bleeding microdrill holes, they dissolved so rapidly that they instantaneously lost their rigid properties (unpublished observations). These implants rehydrated too rapidly to permit controlled delivery and therefore failed the handling test. Implants with chitosan-HCl alone (5 or 10 mg/mL), or chitosan with dextran-5 lyoprotectant rehydrated slowly in the bleeding drilled defect (Fig. 1J). FD-chitosan-HCl alone was sufficient to induce subchondral angiogenesis and bone remodeling at day 21 post-operative (Fig. 1K–M), features of a therapeutic guided subchondral regeneration response [30]. Therefore, the chitosan-HCl pH 2.5 formulation was selected as a prototype implant for testing in skeletally aged sheep.

3.2. Aged sheep SMS cartilage repair model and acute implant residency

The effect of chitosan dose *in vivo* is rarely studied, and the dose effect is largely unknown. Therefore, we designed a cartilage repair study in an aged sheep SMS model using 3 different doses of FD-chitosan (Fig. 2A). We elected to use 80% DDA chitosan at 85 kDa (Table 1), because a presolidified chitosan/blood implant containing 10 kDa chitosan was reported to have no detectable effects on SMS articular cartilage repair in a previous sheep study [44], while a presolidified chitosan/blood implant containing 150 kDa chitosan with a presumably slower clearance rate elicited neocartilage tissue in sheep Jamshidi biopsy osteochondral defects [33]. Microdrill holes were created in a full-thickness cartilage defect in the weight-bearing medial condyle and observed to slowly fill with subchondral blood (Fig. 2B). In treated defects, blood and irrigation fluid were aspirated prior to placing one FD-chitosan implant in each drill hole, at one dose per proximal-to-distal row (Fig. 2C, Table 1). Implant treatment added an average 7.3 min to the arthrotomy and BMS procedure (control defect: 27.5 ± 11.8 min, treated defect: 34.8 ± 7.2 min, incision to suture).

After 1 day of repair, blood clot filled all microdrill holes in control and treated defects (Fig. 2D and E). Drill holes with no implant showed no fluorescence (Fig. 2F), while chitosan microparticles containing fluorescent chitosan tracer were visualized in the drilled defect (Fig. 2G). Histology of day 1 subchondral blood clots showed that the FD-chitosan had dispersed as microparticles in the bone-derived blood clot (Fig. 2H–J). In serial unstained sections through the drill holes, chitosan particles were detected near the top of the bone-derived blood clots. All 3 implant doses were retained in the drill holes with variable amounts of resident chitosan microparticles.

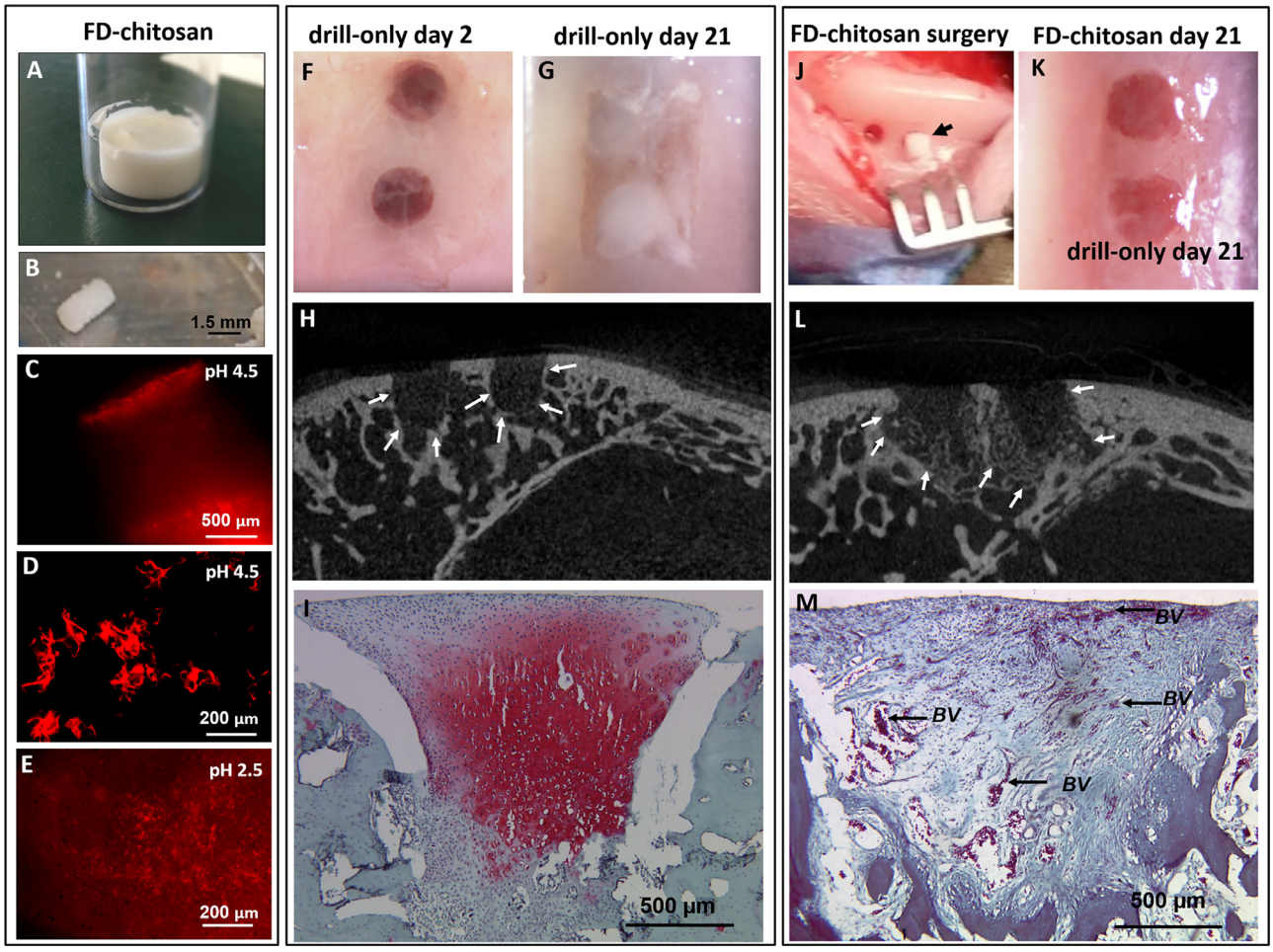

Fig. 1. FD-chitosan formulation screening *in vitro* and *in vivo* in a rabbit SMS model. FD-chitosan macroscopic appearance as a (A) cake and (B) cored implant cylinder and (C–E) microscopic appearance of three different implants containing fluorescent RITC-chitosan tracer at 1 h post-coagulation in human blood plasma fibrin clot (C–E: red signal is RITC-chitosan). (F–M) show representative data from formulation testing in a rabbit model for control drill-only defects (F–I) and chitosan-HCl pH 2.5 implant-treated drill defects (J–M). (F, G, J, K) Drill hole macroscopic appearance at the indicated time points, with matching day 21 sagittal micro-CT images of (H) drill-only and (L) FD-chitosan pH 2.5-treated, and (I, M) histostained sagittal cryosections of osteochondral repair tissues from control (I, Saf-O, non-integrated fibrocartilage) and chitosan-HCl pH 2.5-treated drill holes (M, Gomori trichrome angiogenic repair tissue). Scale bars are as indicated. *Abbreviations and Symbols:* (J) black arrow: FD-chitosan implant; (M) BV: blood vessel; (H and L) white arrows: perimeter of the drill hole (H) and remodeled drill hole (L).

3.3. Sheep microdrill holes undergo bone resorption at 3 months and bone repair by 9 months

Micro-CT measures of residual microdrill hole area showed that initial drill holes had an overall cylindrical hole shape with an average 1.9 mm^2 cross-sectional area that expanded at 3 months post-operative to 3.4 mm^2 (control) and 4.0 mm^2 (treated), and shrank to 0.90 mm^2 (control and treated) at 9 months (Fig. 3).

These data revealed a “wound bloom” effect, where initial drill holes became larger ($p<0.0001$, day 1 *vs* 3 months, Fig. 3) before healing over with bone ($p<0.05$, day 1 *vs* 9 months, Fig. 3). After 3 months of repair, implant-treated microdrill holes had a different shape than control holes, with more bone resorption in the deeper area of treated holes (Fig. 3). Interestingly, residual RITC-chitosan deposits were sporadically observed deeper in several holes in histological sections at 3 months post-operative (*unpublished observations*).

After 9 months of repair, except for one out of 5 sheep with residual unmineralized bone holes in both knees, most drill holes were healed over with mineralized tissue, with a significant narrowing of the drill hole area compared to day 1 and 3 months (Fig. 3). At the top of the drill hole (the osteochondral junction), only implant-treated drill holes showed significant bone repair compared to day 1 ($p = 0.029$, Fig. 3). Residual holes at 9 months consisted mainly of calcifying cartilage or callus at the top of the bone hole and subchondral cysts deeper in the drill hole. These data showed that microdrilling induced bone resorption around the drill hole edges at 3 months followed by mineralized bone repair, with a more complete subchondral bone plate repair in treated drill holes than controls.

3.4. Sheep 3 month and 9 month cartilage repair outcomes

At 3 months post-operative, cartilage defects were largely devoid of macroscopic soft tissue (Fig. 4A) except for one control proximal area, and one defect area treated with 20 mg/mL chitosan implant that were covered with pearly white tissue (arrow, Fig. 4F, treated defect contralateral to the control defect shown in Fig. 4A). Histologically, repair tissues at 3 months post-operative were heterogeneous with many drill holes containing angiogenic tissue at the surface. Callus, a type of mineralizing cartilage, was detected in 55% of control bone holes and 40% of treated holes (non-significant difference, Fig. 4B–D *vs* 4G–I).

Many treated drill holes contained angiogenic granulation tissue and new woven bone (Fig. 4G and H). Chondroinduction was identified as the presence of Saf-O-stained tissue containing chondrocytes at the surface of the drill hole, at or above the osteochondral junction

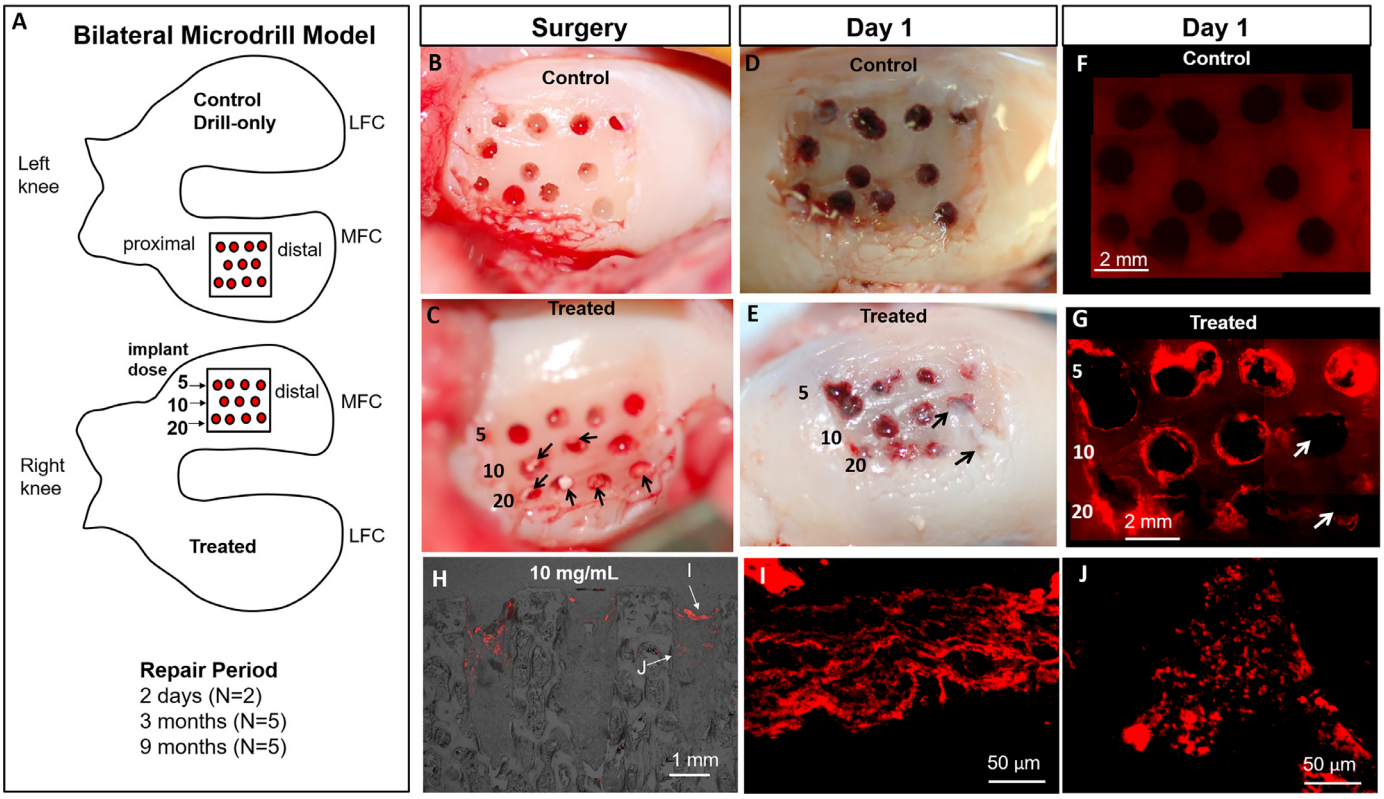

Fig. 2. Chitosan implant delivery and microparticle residency in a bilateral skeletally aged sheep SMS model. (A) schematic of the model and macroscopic appearance at surgery (B, control; C, treated), and at day 1 post-operative (D, control; E, treated). Epifluorescence microscopy of whole defects at day 1 post-operative showed no fluorescence in (F) control drill holes and red RITC-chitosan signal in (G) treated drill holes. Unstained paraffin sections showed RITC-chitosan microparticles resident in treated microdrill holes (H, combined bright field-epifluorescence). Panels (I and J) show treated drill holes at higher-magnification for regions indicated with arrows in panel (H). Arrows in (E, G) show soft tissue covering the holes which blocked visualization of epifluorescent signal. In (A) 5, 10, 20 is the chitosan concentration in mg/mL prior to freeze-dry.

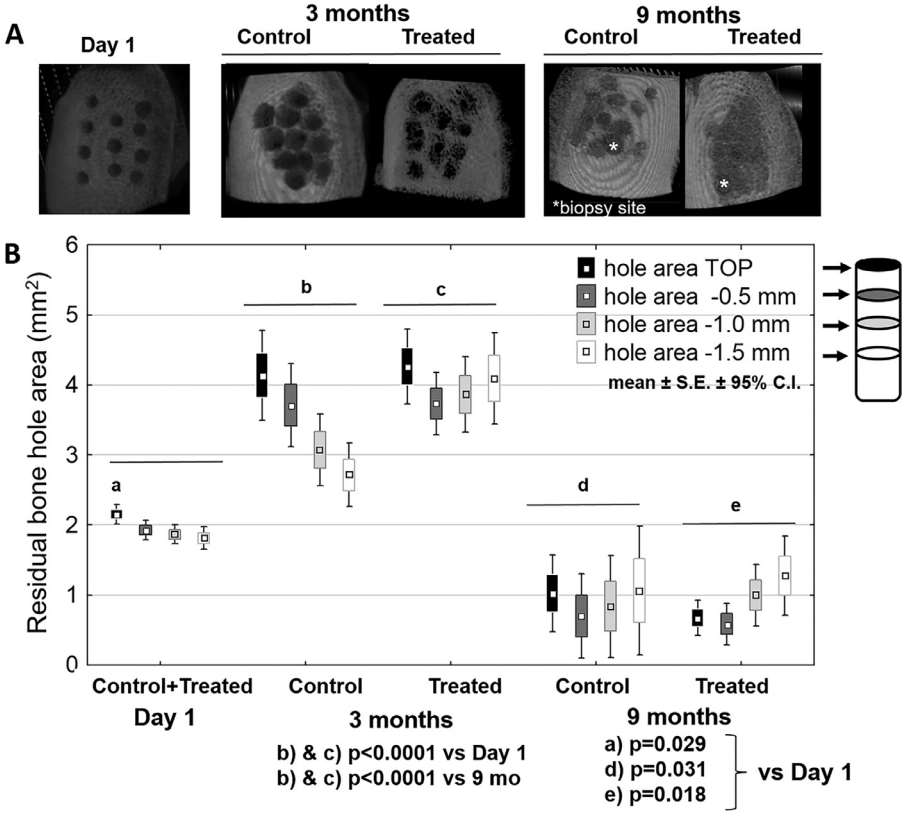

Fig. 3. Micro-CT three-dimensional representative images (A) and calibrated measures of repairing microdrill hole cross-sectional area at different drill hole depths (B) at day 1, 3 months, and 9 months post-operative. Drill holes were approximately 2-fold enlarged at the top of the hole at 3 months then healed over at 9 months, with more complete bone plate repair in FD-chitosan-treated drill holes. The schematic on the right illustrates the 4 depths where drill hole diameter was measured in each drill hole.

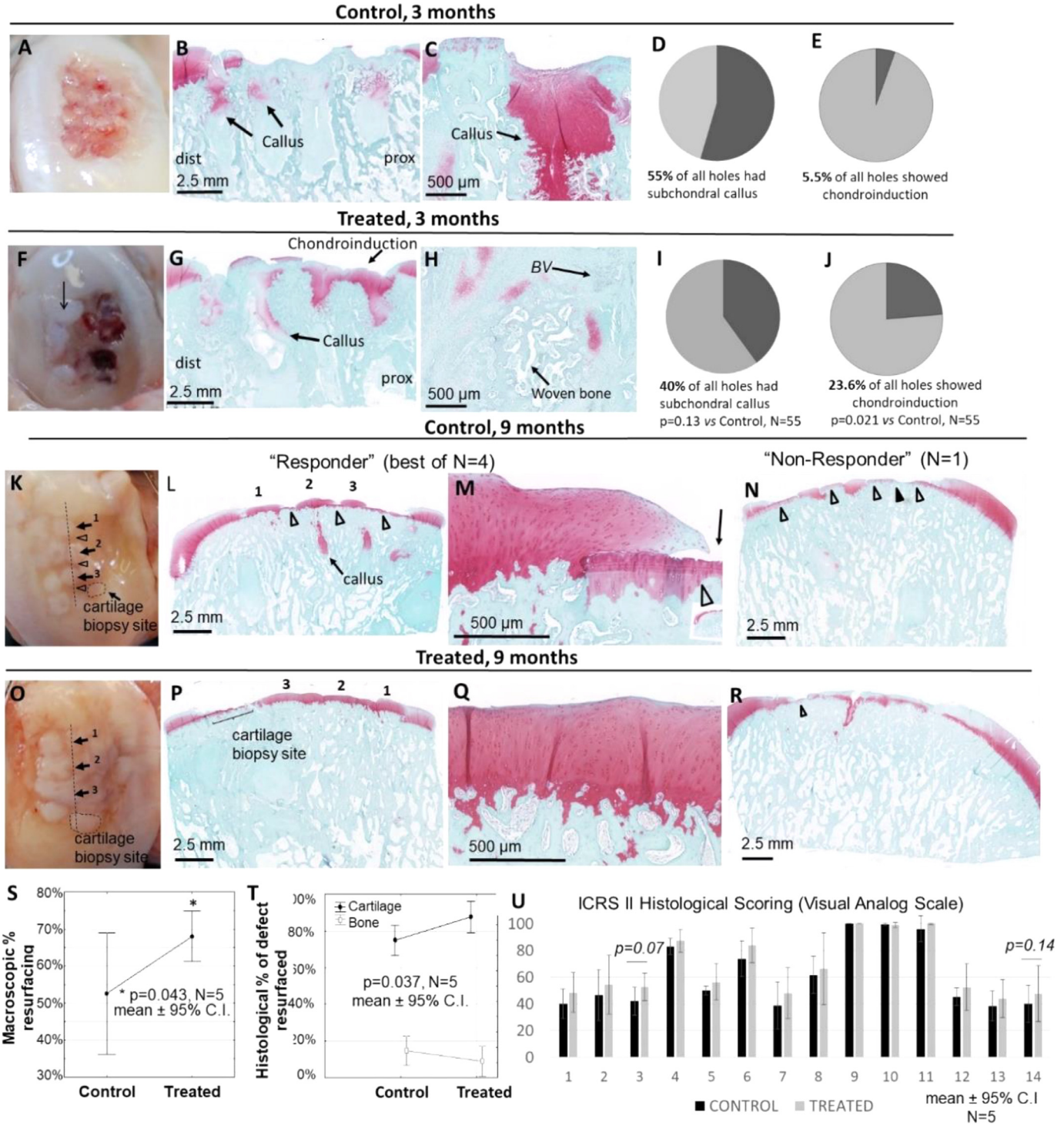

Fig. 4. Macroscopic (A, F, K, O), histomorphometric (D, E, I, J, S, T) and histological (B, C, G, H, L–N, P–R, U) analyses of 3 month and 9 month repair tissues. At 3 months post-operative control subchondral repair tissues (A–E) were predominately callus (D) whereas treated repair tissues (F–J) showed more chondroinduction (J). At 9 months post-operative control cartilage repair tissues (K–N) showed less resurfacing of the cartilage lesion compared to treated cartilage repair tissues (O–T). ICRS-II histological scoring (U) showed that treatment led to higher average scores for all parameters except for parameter 10, with a trend for improved cell morphology (category 3). *Abbreviations and Symbols*: 1, 2, 3 (K, L, O, P) are repaired microdrill holes; K, L, N, R: open arrowheads are exposed bone; black arrowhead (N) is granulation tissue. BV: Blood vessels. Data in S-U: mean ± 95% confidence interval (whiskers) for $N = 5$.

(Fig. 4G). Semi-quantitative histologic scoring revealed a higher incidence of chondroinduction at the surface of implant-treated holes compared to drilling alone ($p = 0.021$, Fig. 4E *vs* Fig. 4J). Sagittal histology sections revealed an interesting proximo-distal healing effect, with a tendency for a more advanced chondrogenesis and greater repair tissue fill in the proximal holes (Fig. 4G).

After 9 months of repair, all defects were resurfaced to a variable degree with a dense white tissue (Fig. 4). In 4 out of 5 sheep, the cartilage repair tissues in both treated and control histology sections stained red with Saf-O and had nascent immature tidemarks at the repair cartilage-repair bone interface (Fig. 4L and M control & P and Q, treated). Treated repair was more integrated than control repair (Fig. 4M *vs* 4Q). In one

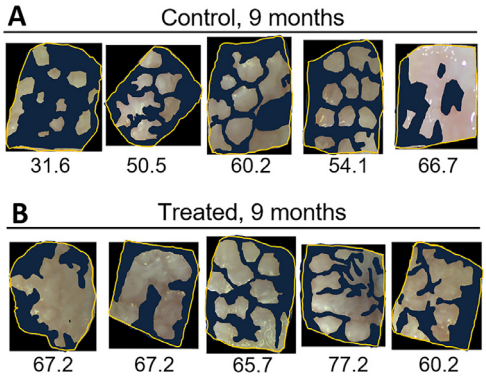

Fig. 5. Raw thresholded image data and corresponding quantitative measures of soft tissue resurfacing from macroscopic images of bilateral defects, with control (A) and the matching contralateral treated defect (B) shown directly below. Greater cartilage repair resurfacing was observed in FD-chitosan treated defects for 4 out of 5 sheep (p = 0.043, mean% resurfacing 67.5% treated *vs* 52.6% control; see Fig. 4S).

sheep with the worst bone repair response (*i.e.*, persisting subchondral un-mineralized callus), the control defect had a large amount of exposed bone (open arrowheads, Fig. 4N) and the treated defect contained GAG-depleted repair tissue (Fig. 4R).

The main effect of implant treatment at 9 months was higher macroscopic % soft tissue resurfacing in 4 out of 5 treated defects (p = 0.043, N = 5, 67.5% treated *vs* 52.6% control, Fig. 4S; Fig. 5). These data were supported by blinded quantitative histomorphometry showing a more integrated cartilage repair tissue (89% *vs* 74%) and less exposed bone (8% *vs* 15%) in treated compared to control cartilage defects (p = 0.037, N = 5, Fig. 4T). Blinded ICRS II histological scoring revealed that treated repair tissues had a modestly higher average score for almost all categories, but due to high variation and low sample number the differences were not significant. A trend for better cell morphology was seen in treated repair tissues (p = 0.07, Category III, Fig. 4U). The ICRS II Overall Score (Category XIV) was 40±14 control and 47±21 treated (p = 0.14, Fig. 4U), which reflected a more complete cartilage repair tissue resurfacing in treated defects. At 9 months post-operative, most menisci had signs of fibrillation with some thinning or occasional small tears (data not shown).

In osteochondral biopsies collected for unconfined compression mechanical tests, repair cartilage was around 2-fold thinner than intact LFC cartilage (p = 0.029, median ~0.5 mm repair *vs* ~0.9 mm LFC, Fig. 5A). The repair tissue equilibrium modulus (Em) and fibril modulus (Ef) were highly variable with control tissues having the lowest mean modulus compared to intact LFC cartilage (control: 0.05 MPa; treated: 0.12 MPa; control LFC: 0.36 MPa; treated LFC: 0.18 MPa; Fig. 6B and C). One control biopsy with a high outlier Em (1.45 MPa) and Ef (25.81) was subsequently identified as being a potential artifact of the white repair tissue in this specimen being subchondral and mostly calcified (Fig. 7).

Most repair tissues had higher median permeability coefficients than LFC cartilage (Fig. 6D), which was consistent with a lower sGAG content in control repair tissues compared to control LFC cartilage (p = 0.036, N = 5, Fig. 6E). Treated repair cartilage had a lower median sGAG content compared to LFC cartilage but due to variability was not significantly different (Fig. 6E). The median sGAG content (±90%C.I.) was 72(10–123) μg/mg wet weight control repair, 91(8–127) μg/mg treated repair, *versus* 156(73–169) μg/mg and 130(89–145) μg/mg for control and treated LFC cartilage, respectively (Fig. 6E).

These data showed that LFC cartilage had no signs of sGAG depletion at 9 months post-operative. Indentation measures carried out over the entire condyle surfaces were used to observe poroelastic mechanical behavior and to measure the force at 100 μm of indentation, otherwise referred to as the structural stiffness (SS@100 μm). SS@100 μm values with high scatter were observed in untreated and treated repair defect sites (0.024–280 N/mm). Repair tissues showed a higher median SS@100 μm (3.9 N/mm) compared to intact cartilage in the MFC (0.5 N/mm for paradefect MFC, 0.4 N/mm for outer MFC), and LFC sites (1.5 N/mm; p<0.005 defect *vs* other regions, Fig. 6F). Co-registration of histological sections and macroscopic images of the indentation sites revealed several contributing factors to the heterogeneous SS@100 μm. Low SS@100 μm values from 0.02 to 0.9 N/mm were frequently observed in very thick hyaline-like repair tissue, and in the paradefect region. The paradefect data were consistent with histology showing sGAG depletion in the paradefect region which means that the tissue had weak mechanical properties and failed to stiffen in response to compression (Fig. 6G). High SS@100 μm values exceeding 7.5 N/mm were mapped to non-resurfaced areas of the defects (calcified cartilage or bone, Fig. 6H). Control defects showed more outlier high SS@100 μm values than treated defects (Fig. 6F) which was consistent with more exposed bone in control defects (Fig. 4S and T). Hyaline-like repair tissues showed poroelastic mechanical features and SS@100 μm values were similar to intact LFC cartilage (Fig. 6I and J). A color map of all SS@100 μm test sites over the cartilage surfaces (Fig. 6J) showed higher stiffness for repair cartilage and LFC cartilage, and lower structural stiffness at 100 μm of indentation in the thicker surrounding MFC cartilage. To summarize, these data showed that treated repair tissues had on average slightly higher sGAG content, slightly lower permeability and less exposed bone according to indentation tests than the repair tissues in defects treated by microdrilling alone.

4. Discussion

This study demonstrated for the first time, to our knowledge, that bioactive biomaterial microparticles delivered into the subchondral bone hematoma can improve the articular cartilage repair outcome in a skeletally aged large animal model. After one day of repair, FD-chitosan microparticles were retained in microdrill holes (Fig. 3). After 3 months of repair, the implant promoted bone remodeling deeper in the drill hole, angiogenic woven bone repair, and chondroinduction at the articular surface (Fig. 4). These responses were followed by a more complete bone plate repair and greater cartilage resurfacing compared to controls. Our study only revealed a trend for improved repair tissue cell morphology due to treatment (Fig. 4U). These collective data support the hypothesis that FD-chitosan microparticles improved the resurfacing of skeletally aged sheep cartilage defects by guiding and altering the subchondral bone wound repair response.

The tissue regeneration rate was very slow in this aged sheep model. Chondral defects were largely unrepaired at 3 months, which may explain resurgent lameness in 3 sheep at 3 months, and meniscal fibrillation at 9 months, both due to unrestricted activity and weight bearing during the entire course of the repair period. Meniscal degeneration could be viewed as a potential adverse effect of BMS in aged knees when there is a very slow repair rate and unrestricted activity. More work is needed to understand tissue regeneration kinetics and to design appropriate rehabilitation programs for older patients admitted to BMS therapy. The aged sheep model is very challenging and the repair response in an acute defect model may not fully mimic the response in chronic defects more typically found in older subjects that can show sclerosis or osteoporosis.

Our study was carried out with 1.5 mm diameter drill holes which are between the 1.0 and 1.8 mm drill hole diameters previously tested by Eldracher et al. [46] in a BMS sheep model using a K-wire. In this former study, smaller holes had a higher quality repair cartilage at 6 months post-operative, as shown by lower average Sellers histologic scores of 19 *vs* 25 (1.0 *vs* 1.8 mm) where 0 is perfect repair and 31 is no repair [46]. Cartilage repair quality was not correlated with any of their measured bone repair parameters at 6 months [46]. In our study, implant treatment had a therapeutic effect on fully restoring the bone plate in

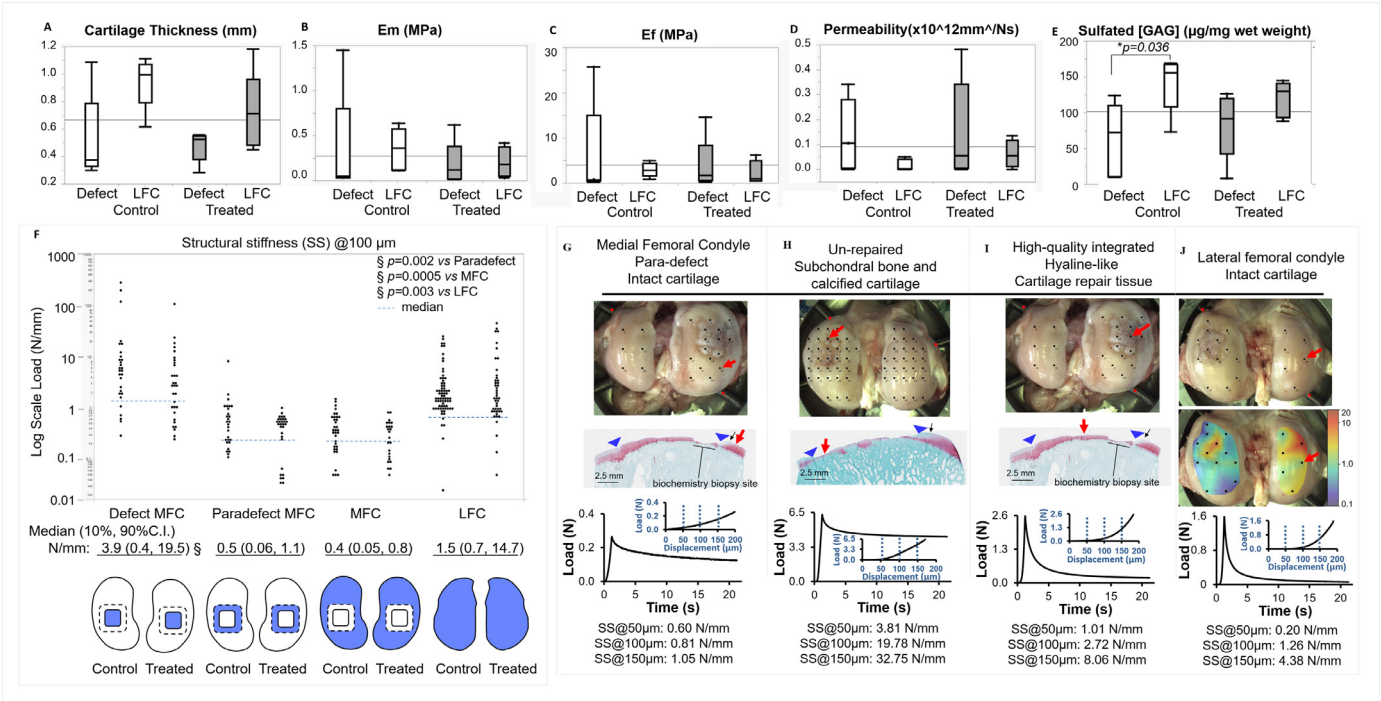

Fig. 6. Mechanical and biochemical analyses of cartilage repair tissues and matching LFC intact cartilage at 9 months post-operative. Osteochondral biopsies with measured (A) cartilage tissue thickness were submitted to unconfined compression to measure (B) Em, (C), Ef and (D) permeability coefficient, (E) sGAG content (µg/mg wet weight) was obtained from adjacent biochemical biopsies. (F) SS@100 µm (N/s) values from automated indentation mapping throughout the regions shown in blue directly below (defect, paradefect MFC, MFC outer regions and LFC). Example stress-relaxation curves from indentation analyses of representative test sites: GAG-depleted paradefect MFC cartilage (G), exposed bone in a defect test site (H), hyaline-like cartilage repair tissue (I, treated defect), and intact LFC cartilage (J; LFC histology was not available therefore the LFC test site is shown on a color map of the interpolated log-scale SS@100 µm data points superposed at 60% transparency over this treated defect knee image (dark blue=0.1 N/mm, red=20 N/mm); In panels (G–J), black dots in macroscopic images: indentation test sites; red arrows: test site shown in the panel; blue arrowheads: cartilage defect boundaries; black arrows: area of sGAG depletion; scale bars are 2.5 mm. *Abbreviations:* LFC: lateral femoral condyle; MFC: medial femoral condyle; SS: structural stiffness; N: Newton; mm: millimeter. Data in (A–E) show the median±quartiles (box)±min/max (whiskers) ($N = 5$) and overall mean (grey horizontal line, $N = 20$). Data in (F) show individual SS@100 µm datapoints collected from 5 distal femurs in the specified test areas ($N = 2$ to $N = 14$ indentation measures per condyle per area). The corresponding median (90% confidence interval) of the combined control and treated test sites is given below.

treated bone holes at 9 months (Fig. 3) that we attribute in part to earlier subchondral angiogenic bone repair. Regeneration of bone at the top of the drill hole permits initiation of chondroinduction at the base of the cartilage lesion, which is especially important to enhance performance of aged stem cells that have a lower capacity for proliferation and chondrogenic differentiation compared to young stem cells [47]. The median sGAG content of repair tissues and LFC in this study (75–100 µg/mg wet weight) were much higher than the depleted sGAG content (0.02–0.06 µg/mg wet weight) reported at 19 months post-operative in a previous sheep study where osteochondral defects were press-fit with stiff bilayer implants composed of polycaprolactone or Chondro-Gide and Orthoss [17].

Although 3 chitosan doses were tested, no dose-effect was evident in any parameter analyzed, apart from tissue outgrowth at 3 months uniquely from 20 mg/mL treated drill holes in 1 out of 5 treated defects. Rehydration of the pH 2.5 FD-chitosan in bleeding subchondral bone could transient acidify the blood clot microenvironment and the impact of this on the therapeutic effect is unknown. We do not expect any acidification to persist very long considering that blood contains many proteins with high buffering capacity. We also observed that microparticles dispersed unevenly in different drill hole clots (Fig. 2H). Homogeneous dispersion of ~1.5 µm diameter chitosan microparticles throughout the hybrid blood clot is preferred compared to aggregated chitosan microparticle deposits. Neutrophils migrate to acetylated chitosan through a leukotriene B_4-sensitive mechanism [48]. Neutrophils attracted to chitosan are important for subsequent attraction of osteoclasts and alternatively activated macrophages that are believed to promote the cartilage repair response during the subchondral healing phase [48]. However a prolonged residence of neutrophil-infiltrated chitosan can delay some of the therapeutic effects of the hybrid chitosan/blood implant such as subchondral angiogenesis, woven bone synthesis, and migration of mesenchymal stem cells towards the cartilage lesion [42,49]. For these reasons, in clinical translation of SMS implant therapies, selecting an optimal dose range and BMS approach will be challenging. Different surgical instruments can produce different levels of subchondral bleeding and bruising [44], which may be related to bone marrow edema that is visualized by magnetic resonance imaging (MRI) in patients with knee pain [50]. The downstream effects of subchondral hematoma are still poorly understood; it is reasonable to presume that disruption of the subchondral vasculature leads to local tissue deprivation of oxygen and nutrients. New blood vessel growth is therefore needed to restore homeostasis following BMS. However, instead of inducing new blood vessel growth, BMS-alone most often stimulates the formation of a mineralizing callus in the area of the bone plate (Fig. 4A; Fig. 7) [29], which could lead to “burning bridges” for subsequent revisions or other cartilage repair treatments [51]. Callus tissue resists remodeling, and some cell-based therapies may require bone remodeling to elicit repair [52]. These collective observations suggest that BMS could be more safely used as a first-line therapy if implants such as FD-chitosan were used to promote angiogenesis and suppress callus formation.

It is remarkable that in this bilateral model of cartilage repair, the main treatment effect was to increase the area of the defect resurfaced

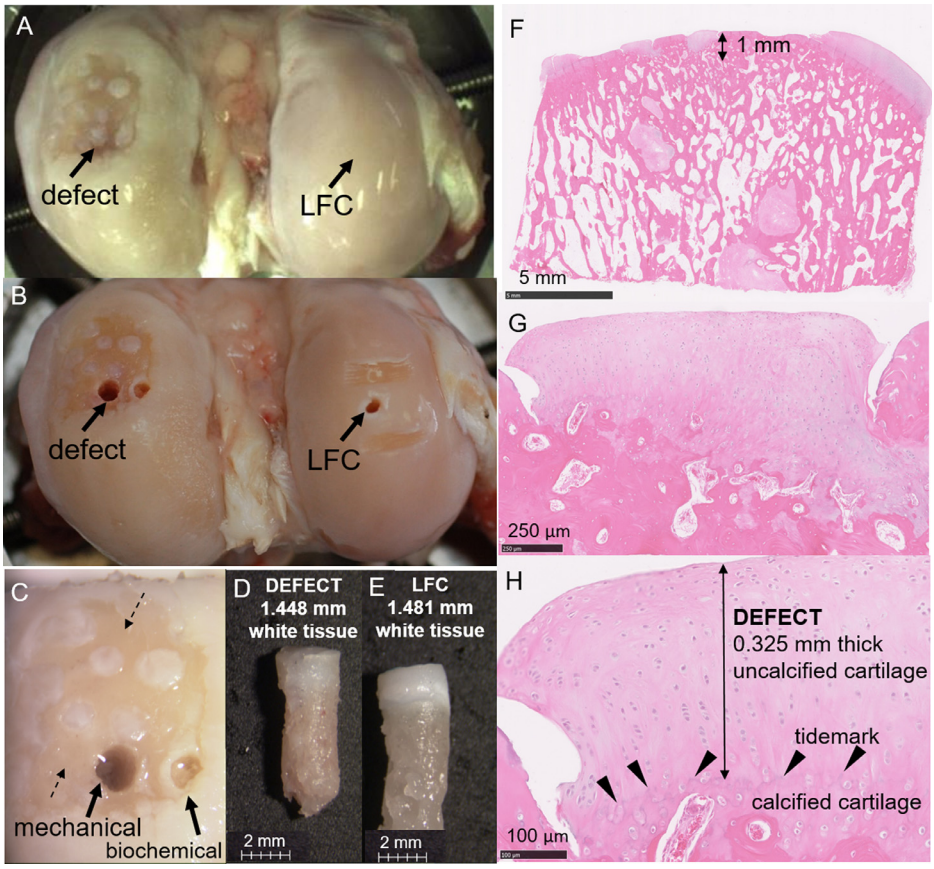

Fig. 7. A single repair cartilage outlier with very high Em and Ef was associated with cartilage repair tissues that were mostly subchondral and partly composed of calcified cartilage. Images of the distal femur of sheep Or26L (untreated control knee) at 9 months post-operative (A) showing "tufts" of repair tissue covering the microdrill holes, (B,C) after the extraction of Jamshidi biopsies for unconfined compression (mechanical) and biopsies for biochemical analysis. Calibrated digital images of biopsies from (D) the defect and (E) the intact LFC were used to measure white cartilage tissue thickness before unconfined compression tests. However H&E stained histology through adjacent repair tissue "tufts" (panels F–H, section collected between the dashed arrows shown in panel C) later revealed that these cartilage tissues were mostly subchondral, contained tidemarks, with only 0.325 mm of uncalcified repair tissue thickness. These data suggest that the high Em and Ef values from the sample in panel D arose from white repair tissue being mostly calcified cartilage.

with cartilage tissue, without significant improvement over controls in sGAG content or mechanical properties. The lack of significant differences is partly due to the low sample number ($N = 5$) which is one of the limitations of this study. Due to the low sample number it is hard to predict whether our biomaterials-based treatment could make a clinical difference for articular cartilage repair, however percent filling of the cartilage lesion with repair tissue was previously singled out as a strong predictor of good clinical outcomes. In a magnetic resonance imaging clinical study of microfracture by Mithoefer et al. [2] ($N = 24$), 100% of patients with "good" fill (67%–100%) showed improvement in their scores for activities for daily living whereas only 40% showed improvement who had "moderate" fill (34%–66%) and only 10% showed improvement with "poor" fill (0%–33%). The percentage resurfacing elicited in our study by FD-chitosan (67.5%) could be comparable to "good" fill in the Mithoefer study while the microdrilling-alone resurfacing (52.6%) is comparable to "moderate" fill, suggesting the potential for a clinically meaningful effect. Other limitations include the lack of histology data for all indentation test sites of LFC samples, and the fact that distinct samples were submitted to biochemistry, histology, and mechanics. Nonetheless, the similar repair tissue properties observed in treated and control bilateral defects reinforce the emerging evidence that each knee has an endogenous osteochondral repair capacity that declines over time [47], that can be improved by the FD-chitosan device.

5. Conclusion

Subchondral chitosan microparticles showed the potential to enhance the volume and basal integration of cartilage repair tissue in aged cartilage lesions treated by bone marrow stimulation. Treated and control cartilage repair tissues had a similar median structural stiffness at 100 µm of indentation, 3.9 N/mm, compared to 1.5 N/mm for intact cartilage in the LFC, and 0.5 N/mm for the thicker intact MFC cartilage tissues surrounding the defect area. Future studies will test the effect of surgical technique (microdrilling *vs* microfracture) and a single chitosan dose.

Declaration of Competing Interest

This work was partly supported by a research grant from Ortho RTi/Prima Quebec. CDH, MDB are on the Board of Directors of Ortho RTi. CDH, MDB, JGM, AC, GC and MBH are shareholders of Ortho RTi. MG and EQ are owners and SS is an employee of Biomomentum. A patent was filed based on some of the findings reported in this study. GP and CHLF have no conflicts to declare.

CRediT authorship contribution statement

Caroline D. Hoemann: Conceptualization, Data curation, Formal analysis, Funding acquisition, Project administration, Supervision, Writing - original draft, Writing - review & editing. **Jessica Guzmán-Morales:** Conceptualization, Formal analysis, Data curation, Writing - original draft, Writing - review & editing. **Geneviève Picard:** Formal analysis, Writing - review & editing. **Gaoping Chen:** Formal analysis, Writing - review & editing. **Daniel Veilleux:** Data curation, Writing - review & editing. **Anik Chevrier:** Data curation, Writing - review & editing. **Sotcheadt Sim:** Formal analysis, Data curation, Writing - review & editing. **Martin Garon:** Data curation, Writing - review & editing. **Eric Quenneville:** Data curation, Writing - review & editing. **Charles-Hubert Lafantaisie-Favreau:** Formal analysis, Writing - review & editing. **Michael D. Buschmann:** Data curation, Writing - review & editing. **Mark B. Hurtig:** Conceptualization, Data curation, Writing - review & editing.

Role of the funding source

Funding sources were not involved in the study design, data collection and analyses, or manuscript submission. Funding was provided by the Canadian Institutes of Health Research (operating grant MOP-133729), Ortho Regenerative Technologies Inc/Prima Quebec (R12 - Advanced Materials).

Data statement

Data will be made available upon reasonable request.

Acknowledgments

We thank Vincent Darras for chitosan molecular weight characterization, Adriana Houle for technical assistance and Julie Tremblay for Quality Assurance.

References

[1] G. Knutsen, J.O. Drogset, L. Engebretsen, T. Grontvedt, V. Isaksen, T.C. Ludvigsen, S. Roberts, E. Solheim, T. Strand, O. Johansen, A randomized trial comparing autologous chondrocyte implantation with microfracture, J. Bone Joint Surg. 89A (10) (2007) 2105–2112.

[2] K. Mithoefer, R.J. Williams, R.F. Warren 3rd, H.G. Potter, C.R. Spock, E.C. Jones, T.L. Wickiewicz, R.G. Marx, The microfracture technique for the treatment of articular cartilage lesions in the knee. A prospective cohort study, J. Bone Joint Surg. 87 (9) (2005) 1911–1920.

[3] G. Knutsen, J.O. Drogset, L. Engebretsen, T. Grontvedt, T.C. Ludvigsen, S. Loken, E. Solheim, T. Strand, O. Johansen, A randomized multicenter trial comparing autologous chondrocyte implantation with microfracture: long-Term follow-up at 14 to 15 years, J. Bone Joint Surg. 98 (16) (2016) 1332–1339 American volume.

[4] X.C. Wei, K. Messner, Maturation-dependent durability of spontaneous cartilage repair in rabbit knee joint, J. Biomed. Mater. Res. 46 (4) (1999) 539–548.

[5] C.G. Pfeifer, M.B. Fisher, V. Saxena, M. Kim, E.A. Henning, D.A. Steinberg, G.R. Dodge, R.L. Mauck, Age-dependent subchondral bone remodeling and cartilage repair in a minipig defect model, Tissue Eng. Part C – Methods 23 (11) (2017) 745–753.

[6] M. Brittberg, A.H. Gomoll, J.A. Canseco, J. Far, M. Lind, J. Hui, Cartilage repair in the degenerative ageing knee: a narrative review and analysis, Acta Orthop. 87 (2016) 26–38.

[7] J.N. Insall, Intra-articular surgery for degenerative arthritis of the knee. A report of the work of the late K. H. Pridie, J. Bone Joint Surg. 49 (2) (1967) 211–228.

[8] J.R. Steadman, W.G. Rodkey, S.B. Singleton, K.K. Briggs, Microfracture technique for full-thickness chondral defects: technique and clinical results, Oper. Tech. Orthop. 7 (4) (1997) 300–304.

[9] K. Mithoefer, R.J. Steadman, Microfracture in football (Soccer) players, Cartilage 3 (1 suppl) (2012) 18S–24S.

[10] J.P. Benthien, P. Behrens, Reviewing subchondral cartilage surgery: considerations for standardised and outcome predictable cartilage remodelling, Int. Orthop. 37 (11) (2013) 2139–2145.

[11] G. Knutsen, L. Engebretsen, T.C. Ludvigsen, J.O. Drogset, T. Grontvedt, E. Solheim, T. Strand, S. Roberts, V. Isaksen, C. Johansen, Autologous chondrocyte implantation compared with microfracture in the knee – a randomized trial, J. Bone Joint Surg. 86A (3) (2004) 455–464.

[12] D.B. Saris, J. Vanlauwe, J. Victor, M. Haspl, M. Bohnsack, Y. Fortems, B. Vandekerckhove, K. Almqvist, et al., Characterized chondrocyte implantation results in better structural repair when treating symptomatic cartilage defects of the knee in a randomized controlled trial *versus* microfracture, Am. J. Sports Med. 36 (2) (2008) 235–246.

[13] G.I. Im, Endogenous cartilage repair by recruitment of stem cells, Tissue Eng. Part B – Rev. 22 (2) (2016) 160–171.

[14] R. Langer, J.P. Vacanti, Tissue engineering, Science 260 (5110) (1993) 920–926.

[15] V. Karageorgiou, D. Kaplan, Porosity of 3D biomaterial scaffolds and osteogenesis, Biomaterials 26 (27) (2005) 5474–5491.

[16] B. Sharma, C.G. Williams, T.K. Kim, D.N. Sun, A. Malik, M. Khan, K. Leong, J.H. Elisseeff, Designing zonal organization into tissue-engineered cartilage, Tissue Eng. 13 (2) (2007) 405–414.

[17] J.C. Schagemann, N. Rudert, M.E. Taylor, S. Sim, E. Quenneville, M. Garon, M. Klinger, M.D. Buschmann, H. Mittelstaedt, Bilayer implants: electromechanical assessment of regenerated articular cartilage in a sheep model, Cartilage 7 (4) (2016) 346–360.

[18] C. Erggelet, K. Neumann, M. Endres, K. Haberstroh, M. Sittinger, C. Kaps, Regeneration of ovine articular cartilage defects by cell-free polymer-based implants, Biomaterials 28 (36) (2007) 5570–5580.

[19] E. Kon, G. Filardo, M. Delcogliano, M. Fini, F. Salamanna, G. Giavaresi, I. Martin, M. Marcacci, Platelet autologous growth factors decrease the osteochondral regeneration capability of a collagen-hydroxyapatite scaffold in a sheep model, BMC Musculoskelet. Disord. 11 (1) (2010) 220.

[20] M. Hamanishi, T. Nakasa, N. Kamei, H. Kazusa, G. Kamei, M. Ochi, Treatment of cartilage defects by subchondral drilling combined with covering with atelocollagen membrane induces osteogenesis in a rat model, J. Orthop. Sci. 18 (4) (2013) 627–635.

[21] F. Streitparth, P. Schoettle, K. Schlichting, H. Schell, F. Fischbach, T. Denecke, G.N. Duda, R.J. Schroeder, Osteochondral defect repair after implantation of biodegradable scaffolds: indirect magnetic resonance arthrography and histopathologic correlation, Acta Radiol. 50 (7) (2009) 765–774.

[22] J. Verhaegen, S. Clockaerts, G. Van Osch, J. Somville, P. Verdonk, P. Mertens, TruFit plug for repair of osteochondral defects-where is the evidence? Systematic review of literature, Cartilage 6 (1) (2015) 12–19.

[23] A. Abarrategi, Y. Lopiz-Morales, V. Ramos, A. Civantos, L. Lopez-Duran, F. Marco, J.L. Lopez-Lacomba, Chitosan scaffolds for osteochondral tissue regeneration, J. Biomed. Mater. Res. Part A 95A (4) (2010) 1132–1141.

[24] S.A. Lietman, S. Miyamoto, P.R. Brown, N. Inoue, A.H. Reddi, The temporal sequence of spontaneous repair of osteochondral defects in the knees of rabbits is dependent on the geometry of the defect, J. Bone Joint Surg. 84 (11) (2001) 600–606.

[25] P. Orth, M. Cucchiarini, G. Kaul, M.F. Ong, S. Gräber, D.M. Kohn, H. Madry, Temporal and spatial migration pattern of the subchondral bone plate in a rabbit osteochondral defect model, Osteoarthr. Cartil. 20 (10) (2012) 1161–1169.

[26] M. Yokota, K. Yasuda, N. Kitamura, K. Arakaki, S. Onodera, T. Kurokawa, J.P. Gong, Spontaneous hyaline cartilage regeneration can be induced in an osteochondral defect created in the femoral condyle using a novel double-network hydrogel, BMC Musculoskelet. Disord. 14 (27) (2013), doi:10.1186/1471-2474-14-27.

[27] J. Guzman-Morales, C.H. Lafantaisie-Favreau, G. Chen, C.D. Hoemann, Subchondral chitosan/blood implant-guided bone plate resorption and woven bone repair is coupled to hyaline cartilage regeneration from microdrill holes in aged rabbit knees, Osteoarthr. Cartil. 22 (2) (2014) 323–333.

[28] W. Zhang, Q. Lian, D. Li, K. Wang, D. Hao, W. Bian, J. He, Z. Jin, Cartilage repair and subchondral bone migration using 3D printing osteochondral composites: a one-year-period study in rabbit trochlea, Biomed. Res. Int. 2014 (2014) 16.

[29] A. Beck, D.J. Murphy, R. Carey-Smith, D.J. Wood, M.H. Zheng, Treatment of articular cartilage defects with microfracture and autologous matrix-induced chondrogenesis leads to extensive subchondral bone cyst formation in a sheep model, Am. J. Sports Med. 44 (10) (2016) 2629–2643.

[30] A. Chevrier, C.D. Hoemann, J. Sun, M.D. Buschmann, Chitosan-glycerol phosphate/blood implants increase cell recruitment, transient vascularization and subchondral bone remodeling in drilled cartilage defects, Osteoarthr. Cartil. 15 (3) (2007) 316–327.

[31] Y.M. Yen, B. Cascio, L. O'Brien, S. Stalzer, P.J. Millett, J.R. Steadman, Treatment of osteoarthritis of the knee with microfracture and rehabilitation, Med. Sci. Sports Exerc. 40 (2) (2008) 200–205.

[32] C.D. Hoemann, Y. Gosselin, H.M. Chen, J. Sun, M.B. Hurtig, A. Carli, W.D. Stanish, Characterization of initial microfracture defects in human condyles, J. Knee Surg. 26 (5) (2013) 347–355.

[33] A.D. Bell, V. Lascau-Coman, J. Sun, G. Chen, M.W. Lowerison, M.B. Hurtig, C.D. Hoemann, Bone-Induced chondroinduction in sheep jamshidi biopsy defects with and without treatment by subchondral chitosan-blood implant: 1-Day, 3-Week, and 3-Month repair, Cartilage 4 (2) (2013) 131–143.

[34] G. Chen, J. Sun, V. Lascau-Coman, A. Chevrier, C. Marchand, C.D. Hoemann, Acute osteoclast activity following subchondral drilling is promoted by chitosan and associated with improved cartilage tissue integration, Cartilage 2 (2) (2011) 173–185.

[35] Y.J. Seol, J.Y. Lee, Y.-J. Park, Y. Ku, I.-C. Rhyu, S.-J. Lee, S.-B. Han, C.-P. Chung, Chitosan sponges as tissue engineering scaffolds for bone formation, Biotechnol. Lett. 26 (13) (2004) 1037–1041.

[36] C.R. Almeida, T. Serra, M.I. Oliveira, J.A. Planell, M.A. Barbosa, M. Navarro, Impact of 3-D printed PLA- and chitosan-based scaffolds on human monocyte/macrophage responses: unraveling the effect of 3-D structures on inflammation, Acta Biomater. 10 (2) (2014) 613–622.

[37] O. Ma, M. Lavertu, J. Sun, S. Nguyen, M.D. Buschmann, F.M. Winnik, C.D. Hoemann, Precise derivatization of structurally distinct chitosans with rhodamine b isothiocyanate, Carbohydr. Polym. 72 (4) (2008) 616–624.

[38] A. Contreras-García, N.L. D'Elía, M. Desgagné, C.-H. Lafantaisie-Favreau, G.-E. Rivard, J.-C. Ruiz, M.R. Wertheimer, P. Messina, C.D. Hoemann, Synthetic anionic surfaces can replace microparticles in stimulating burst coagulation of blood plasma, Colloids Surf. B: Biointerfaces 175 (2019) 596–605.

[39] C. Kilkenny, W.J. Browne, I.C. Cuthill, M. Emerson, D.G. Altman, Improving bioscience research reporting: the ARRIVE guidelines for reporting animal research, PLoS Biol. 8 (6) (2010) e1000412.

[40] C. Pauli, S.P. Grogan, S. Patil, S. Otsuki, A. Hasegawa, J. Koziol, M.K. Lotz, D.D. D'Lima, Macroscopic and histopathologic analysis of human knee menisci in aging and osteoarthritis, Osteoarthr. Cartil. 19 (9) (2011) 1132–1141.

[41] C.D. Hoemann, J. Sun, V. Chrzanowski, M.D. Buschmann, A multivalent assay to detect glycosaminoglycan, protein, collagen, RNA, and DNA content in milligram samples of cartilage or hydrogel-based repair cartilage, Anal. Biochem. 300 (1) (2002) 1–10.

[42] C.H. Lafantaisie-Favreau, J. Guzman-Morales, J. Sun, G.P. Chen, A. Harris, T.D. Smith, A. Carli, J. Henderson, W.D. Stanish, C.D. Hoemann, Subchondral presolidified chitosan/blood implants elicit reproducible early osteochondral wound-repair responses including neutrophil and stromal cell chemotaxis, bone resorption and repair, enhanced repair tissue integration and delayed matrix deposition, BMC Musculoskelet. Disord. 14 (2013), doi:10.1186/1471-2474-14-27.

[43] P. Mainil-Varlet, T. Aigner, M. Brittberg, P. Bullough, A. Hollander, E. Hunziker, R. Kandel, S. Nehrer, K. Pritzker, S. Roberts, E. Stauffer, Histological assessment of cartilage repair – a report by the histology endpoint committee of the international cartilage repair society (ICRS), J. Bone Joint Surg. 85A (2003) 45–57.

[44] A.D. Bell, M.B. Hurtig, E. Quenneville, G.-É. Rivard, C.D. Hoemann, Effect of a rapidly degrading presolidified 10kDa chitosan/blood implant and subchondral marrow stimulation surgical approach on cartilage resurfacing in a sheep model, Cartilage 8 (4) (2017) 417–431.
[45] J. Soulhat, M.D. Buschmann, A. Shirazi-Adl, A fibril-network-reinforced biphasic model of cartilage in unconfined compression, J. Biomech. Eng. – Trans. ASME 121 (3) (1999) 340–347.
[46] M. Eldracher, P. Orth, M. Cucchiarini, D. Pape, H. Madry, Small subchondral drill holes improve marrow stimulation of articular cartilage defects, Am. J. Sports Med. 42 (11) (2014) 2741–2750.
[47] G. Dwivedi, A. Chevrier, C.D. Hoemann, M.D. Buschmann, Bone marrow progenitor cells isolated from young rabbit trochlea are more numerous and exhibit greater clonogenic, chondrogenic, and osteogenic potential than cells isolated from condyles, Cartilage 9 (4) (2018) 378–390.
[48] C.D. Hoemann, G. Chen, C. Marchand, J. Sun, N. Tran-Khanh, A. Chevrier, M. Thibault, M.G.J. Fernandes, P.E. Poubelle, M.S. Shive, M. Centola, H. El-Gabalawy, Scaffold-guided subchondral bone repair: implication of neutrophils and alternatively activated arginase-1+ macrophages, Am. J. Sports Med. 38 (9) (2010) 1845–1856.
[49] C. Mathieu, A. Chevrier, V. Lascau-Coman, G.E. Rivard, C.D. Hoemann, Stereological analysis of subchondral angiogenesis induced by chitosan and coagulation factors in microdrilled articular cartilage defects, Osteoarthr. Cartil. 21 (6) (2013) 849–859.
[50] F.W. Roemer, R. Frobell, D.J. Hunter, M.D. Crema, W. Fischer, K. Bohndorf, A. Guermazi, MRI-detected subchondral bone marrow signal alterations of the knee joint: terminology, imaging appearance, relevance and radiological differential diagnosis, Osteoarthr. Cartil. 17 (9) (2009) 1115–1131.
[51] T. Minas, A.H. Gomoll, R. Rosenberger, R.O. Royce, T. Bryant, Increased failure rate of autologous chondrocyte implantation after previous treatment with marrow stimulation techniques, Am J. Sports Med. 37 (2009) 902–908.
[52] H.A. Breinan, T. Minas, H. Hsu, S. Nehrer, S. Shortkroff, M. Spector, Autologous chondrocyte implantation in a canine model: change in composition of reparative tissue with time, J. Orthop. Res. 19 (3) (2001) 482–492.